Investigation of LPG-SPR sensors using the finite element method and eigenmode expansion method

Yue Jing He*

Department of Electronic Engineering, National Chin-Yi University of Technology, Taichung, Taiwan
**yuejing@ncut.edu.tw*

Abstract: As compared to the well-known traditional couple-mode theory, in this study, we proposed a visual, graphical, and simple numerical simulation method for long-period fiber-grating surface-plasmon-resonance (LPG-SPR) sensors. This method combines the finite element method and the eigenmode expansion method. The finite element method was used to solve for the guided modes in fiber structures, including the surface plasmon wave. The eigenmode expansion method was used to calculate the power transfer phenomenon of the guided modes in the fiber structure. This study provides a detailed explanation of the key reasons why the periodic structure of long-period fiber-grating (LPG) can achieve significantly superior results for our method compared to those obtained using other numerical methods, such as the finite-difference time-domain and beam propagation methods. All existing numerical simulation methods focus on large-sized periodic components; only the method established in this study has 3D design and analysis capabilities. In addition, unlike the offset phenomenon of the design wavelength λ_D and the maximum transmission wavelength λ_{max} of the traditional coupled-mode theory, the method established in this study has rapid scanning LPG period capabilities. Therefore, during the initial component design process, only the operating wavelength must be set to ensure that the maximum transmission wavelength of the final product is accurate to the original setup, for example, λ = 1550 nm. We verified that the LPG-SPR sensor designed in this study provides a resolution of ~-45 dB and a sensitivity of ~27000 nm/RIU (refractive index unit). The objective of this study was to use the combination of these two numerical simulation methods in conjunction with a rigorous, simple, and complete design process to provide a graphical and simplistic simulation technique that reduces the learning time and professional threshold required for research and applications of LPG-SPR sensors.

OCIS codes: (240.6680) Surface plasmons; (350.2770) Gratings; (240.6690) Surface waves.

References and links

1. J. Homola, "Optical fiber sensor based on surface plasmon excitation," Sens. Actuators B Chem. **29**(1-3), 401–405 (1995).
2. R. Slavík, J. Homola, and J. Čtyroký, "Single-mode optical fiber surface plasmon resonance sensor," Sens. Actuators B Chem. **54**(1-2), 74–79 (1999).
3. S.-M. Tseng, K.-Y. Hsu, H.-S. Wei, and K.-F. Chen, "Analysis and experiment of thin metal-clad fiber polarizer with index overlay," IEEE Photon. Technol. Lett. **9**(5), 628–630 (1997).
4. Ó. Esteban, R. Alonso, M. C. Navarrete, and A. González-Cano, "Surface plasmon excitation in fiber-optical sensors: a novel theoretical approach," J. Lightwave Technol. **20**(3), 448–453 (2002).
5. S. Patskovsky, A. V. Kabashin, M. Meunier, and J. H. Luong, "Silicon-based surface plasmon resonance sensing with two surface plasmon polariton modes," Appl. Opt. **42**(34), 6905–6909 (2003).
6. S. Patskovsky, A. V. Kabashin, M. Meunier, and J. H. Luong, "Properties and sensing characteristics of surface-plasmon resonance in infrared light," J. Opt. Soc. Am. A **20**(8), 1644–1650 (2003).

#179197 - $15.00 USD Received 2 Nov 2012; revised 10 Jan 2013; accepted 15 Jan 2013; published 3 Jun 2013

7. A. J. C. Tubb, F. P. Payne, R. B. Millington, and C. R. Lowe, "Single-mode optical fibre surface plasma wave chemical sensor," Sens. Actuators B Chem. **41**(1-3), 71–79 (1997).
8. S. Maruo, O. Nakamura, and S. Kawata, "Evanescent-wave holography by use of surface-plasmon resonance," Appl. Opt. **36**(11), 2343–2346 (1997).
9. Y. J. He, Y. L. Lo, and J. F. Huang, "Optical-fiber surface-plasmon-resonance sensor employing long-period fiber grating in multiplexing," J. Opt. Soc. Am. B **23**(5), 801–811 (2006).
10. E. D. Palik, *Handbook of Optical Constants of Solids* (Academic Press, 1985).
11. D. Sun, J. Manges, Xingchao Yuan, and Z. Cendes, "Spurious modes in finite-element methods," IEEE Antennas Propag. Mag. **37**(5), 12–24 (1995).
12. C. H. Herry and Y. Shani, "Analysis of mode propagation in optical waveguide devices by Fourier expansion," IEEE J. Quantum Electron. **27**(3), 523–530 (1991).
13. G. Sztefka and H. P. Nolting, "Bidirectional eigenmode Propagation for Large refractive index steps," IEEE Photon. Technol. Lett. **5**(5), 554–557 (1993).
14. D. F. G. Gallagher and T. P. Felici, "Eigenmode expansion methods for simulation of optical propagation in photonics-Pros and cons," Proc. SPIE **4987**, 69–82 (2003).
15. T. Erdogan, "Cladding-mode resonances in short and long period fiber grating filters," J. Opt. Soc. Am. A **14**(8), 1760–1773 (1997).
16. T. Erdogan, "Fiber grating spectra," J. Lightwave Technol. **15**(8), 1277–1294 (1997).

1. Introduction

To minimize the size of surface plasmon resonance (SPR) sensors, the configuration involving a bent, polished, single-mode optical fiber and a thin metallic film has been recommended for the past decade [1–4]. This structure is similar to the Kretschmann configuration in its excitation of a surface plasmon wave (SPW). According to geometric optics theory, the trajectory of a core mode, solved using the Maxwell equations, forms a ray angle at the core-cladding interface [5–8]. In this structure, variation in the refractive index of the analyte is determined by monitoring changes in the transmitted optical power at a fixed wavelength or changes in the wavelength where the resonance occurs. This type of structure has become common because it depends substantially on the refractive index of the surrounding medium. Most notably, the cylindrical symmetry of the fiber in this configuration is not real because of the presence of a side-polished layer. Therefore, modeling the waveguide properties rigorously is extremely difficult. All the theoretical models that have been proposed use the pseudo-TM mode of unpolished fiber to analyze the bent, polished structure. Thus, these models exhibit some degree of error in analysis. Recently, a new type of optical-fiber SPR sensor based on a thin metallic film, which is deposited uniformly on the cladding of an optical fiber, and long-period fiber grating have been presented. This sensor (LPG-SPR sensor) employs long-period fiber grating and an appropriate period to couple a core mode to a co-propagating cladding mode that can excite a SPW, and monitors the change in the core mode power transmitted at a fixed wavelength or changes in the wavelength where the resonance occurs to identify variations in the refractive index of analyte.

Presently, the traditional unconjugated form of coupled-mode theory is one of the techniques most commonly used in studies of LPG-SPR sensor characteristics and related applications [9]. For scholars new to the LPG-SPR sensor field, learning this theory is critical and indispensable for understanding the physical concepts of LPG-SPR sensors. Evidently, the traditional unconjugated form of coupled-mode theory plays a pivotal role in understanding the characteristics of LPG-SPR sensors. Below, we use three brief descriptions to introduce how the traditional unconjugated form of coupled-mode theory can be employed to perform LPG-SPR sensor analysis and design.

1.1 Defining the LPG-SPR sensor structure and solving for guided modes

The geometric structure of general LPG-SPR sensors comprises four layers of media: a core layer, cladding layer, metallic layer, and analyte. The material used for the metallic layer in this study was gold. The complex refractive index of gold was obtained from the *Handbook of Optical Constants of Solids* (Academic Press, 1985), and its precise wavelength-dependent fit to the data within was determined using a cubic spline algorithm [10]. The relationship between the refractive index and the wavelength of gold is shown in Fig. 1. In addition, the related parameters of the various media layers were a_1 = 2.25 μm and a_2 = 18 μm, and the

#179197 - $15.00 USD Received 2 Nov 2012; revised 10 Jan 2013; accepted 15 Jan 2013; published 3 Jun 2013

thickness of the metallic layers was 0.02 μm, a_3 = 18.02 μm, n_1 = 1.45, n_2 = 1.43, n_3 = 0.56246309 + j9.840798407 (λ = 1550 nm), and n_4 = 1.4. A schematic diagram is shown in Fig. 2 below. Notably, the ideal radius of the tested layers should be infinite.

After determining the cross-section geometric structure of the fiber, we employed the Maxwell equations combined with boundary conditions and solutions to dispersion relation equations. Finally, we obtained all the guided modes that existed in the structure, which included the SPW and effective refractive index that corresponded to each mode n_{eff}^{v} [9]. Simply explained from a purely mathematical perspective, modes are solutions to differential equations that can satisfy specific boundary conditions. Unless otherwise specified, in this study, we only analyzed single-mode fibers. That is, we obtained single-core modes n_{eff}^{core} ($n_2 < n_{eff}^{core} < n_1$) and approximately infinite cladding modes $n_{eff}^{cladding}$ ($n_3 < \mathrm{Re}(n_{eff}^{cladding}) < n_2$).

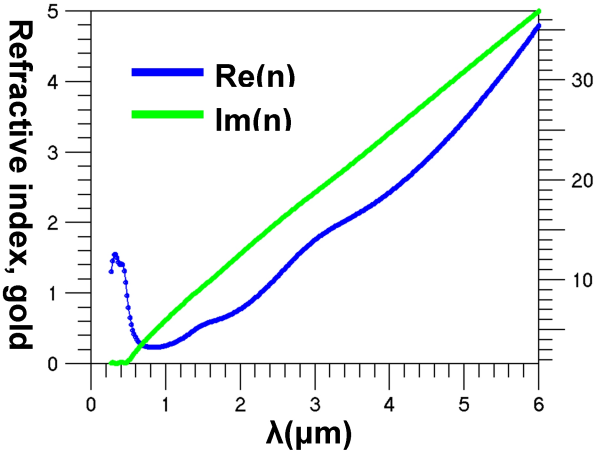

Fig. 1. The relationship between the refractive index and the wavelength of gold.

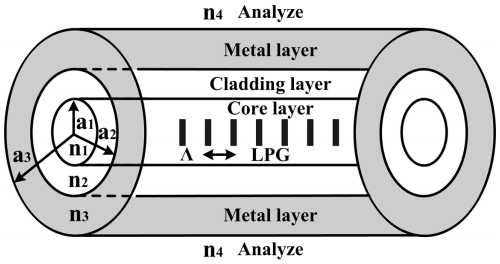

Fig. 2. The geometric structure and parameter schematic of typical fibers and LPG-SPR sensors.

1.2 Defining the mathematical model of fiber grating and explaining the equation of the unconjugated form of the coupled-mode

For LPG production, we first selected a single-mode with fiber photosensitive materials for the core layer. Then we used ultraviolet light to irradiate the amplitude mask with specific periods to allow the power to provide constructive and destructive interferences on the single-mode fiber and to further change the core layer refractive index. The mathematical model for uniform fiber grating is expressed as follows:

$$n_1(z) = n_1 + \delta n\left[1+\cos(\frac{2\pi}{\Lambda}z)\right]. \quad (1)$$

#179197 - $15.00 USD Received 2 Nov 2012; revised 10 Jan 2013; accepted 15 Jan 2013; published 3 Jun 2013

Here, δn is the peak induced-index change, and Λ is the optical fiber-grating period. From a mathematical perspective, before fiber grating occurred, all the modes in the fiber waveguides were orthogonal to each other. That is, during the entire propagation process, power between the modes could not be exchanged or coupled. However, after the LPG was written to the core layer, it generated a power perturbation effect between the modes. Appropriately designed LPG periods Λ can disturb the orthogonality of the original modes and achieve a power coupling phenomenon. Under the $\delta n << n_1$ condition, the mathematical model of unconjugated coupling among the modes can be expressed as follows [9]:

$$\frac{dA_\mu}{dz} = iA_\nu K_{\nu-\mu} \exp\left[i(\beta_\nu - \beta_\mu)z\right] \tag{2}$$

of which

$$K_{\nu-\mu} = \frac{w}{2} \frac{\Delta\varepsilon \int_{A\infty} (E_r^\nu E_r^\mu + E_\varphi^\nu E_\varphi^\mu) dA - \frac{\Delta\varepsilon}{\Delta\varepsilon + \varepsilon} \int_{A\infty} (E_z^\nu E_z^\mu) dA}{\int_0^{2\pi} \int_0^\infty (E_r^\mu H_\varphi^\mu - E_\varphi^\mu H_r^\mu) dA}. \tag{3}$$

where A_μ and A_ν denote the amplitude of any guiding modes in the fiber, β_μ and β_ν denote the propagation constants of any guiding modes in the fiber, $K_{\nu-\mu}$ represents the coupling coefficients between modes ν and μ, $\Delta\varepsilon$ represents the variation quantity of the dielectric constant caused by the LPG on the core layer, and w is the angular frequency.

1.3 Defining the bar and cross-transmission power spectrum

To analyze the spectral characteristics of LPG-SPR sensors, we defined the bar transmission power and cross-transmission power using the following mathematical equations:

$$t_= = \frac{|R(z)|^2}{|R(0)|^2}, \tag{4}$$

$$t_\times = \frac{|S(z)|^2}{|R(0)|^2}. \tag{5}$$

In layman's terms, the bar transmission power is the self-power ratio of the incident mode HE_{11} after traveling a certain distance (z) and when incidence occurs (z = 0). In other words, for incident mode HE_{11}, after traveling a certain distance (z), if the power can be coupled to other modes, the power ratio of the modes and the incidence (z = 0) HE_{11} denote the cross transmission power. The power spectrum diagram of LPG-SPR sensors can be obtained by using these two parameters and configuring the wavelengths in diagram form.

In the preceding introduction, we have endeavored to analyze and simplify the unconjugated form of coupled-mode theory and provide the most comprehensive introduction to its physical concepts in layman's terms, using as few mathematical equations as possible. Evidently, the traditional unconjugated form of coupled-mode theory is not only a significant mathematical burden for novice learners of LPG-SPR sensors, but its daunting difficulty is also dreaded by application-level designers. Therefore, the main objective of this study was to combine two well-known numerical simulation methods to propose a visual and simplistic simulation technique. A rigorous content design process was employed to reduce the learning time and professional threshold required for research and applications of LPG-SPR sensors.

The remaining content of this study is described as follows: Section 2 provides a brief introduction to theories related to the finite element method (FEM). Regarding numerical methods, the cutting resolution of triangular elements critically affects the correctness of the

#179197 - $15.00 USD Received 2 Nov 2012; revised 10 Jan 2013; accepted 15 Jan 2013; published 3 Jun 2013

modes obtained. From a mathematical perspective, if all the modes obtained are correct, the orthogonal values between the modes must be 0. Thus, we used the reverse-thinking method to determine the allowable orthogonal value, which was 10^{-4}, before adjusting the cutting resolutions to perform simulations. In addition, we also randomly inspected the modes obtained to determine whether they conformed to the relevant norm specifying orthogonal values of less than 10^{-4}.

In Section 3, we introduce theories related to the eigenmode expansion method (EEM). In this section, we provide a detailed explanation of how the eigenmode expansion method allows guided modes to conduct transmissions in LPG-SPR sensor structures. We also specified the main reason why this method is significantly superior to the finite-difference time-domain method and the beam propagation method. However, this numerical method also exhibited accuracy problems. The Fourier series expansion is the main principle that enabled light wave transmissions to be performed using this numerical method. That is, if the number of modes was insufficient during the transfer process, even in non-absorbent media, the total power would decline as the number of implementing Fourier series expansion increased. We used the reverse thinking method to employ different numbers of guided modes to perform transmissions, consider the power lost, and determine the number of guided modes for this study. Here, we must emphasize that for non-absorbent media, the power lost in transmission distances is typically used to determine the sufficient mode quantity. However, that light wave power attenuates with distance in absorbent materials is a natural phenomenon. To determine the power loss caused by the Fourier series expansion, we should consider the original definition of loss. That is, observe the power loss conditions for every position of the Fourier series expansion execution. Because of the presence of gold and the absorbent material used in the structure for this study, when designing and analyzing the LPG-SPR sensor, we checked the power losses of all Fourier series expansion positions according to the basic definition of loss to verify the legitimacy of the eigenmode expansion method.

In Section 4, we summarize the content of Sections 2 and 3 to propose a rigorous, simplistic, and comprehensive design process for analyzing and designing LPG-SPR sensors. In this section, we also present numerous graphical simulation results to visually and simplistically supplement the formulaic and abstract content of the traditional unconjugated form of coupled-mode theory learning.

In the final section, we summarize all the numerical simulation methods proposed in this study, and collate all the data obtained in Section 4, to verify that the method proposed in this study does provide a visual and simplistic simulation technique for large-scale periodic components, and to reduce the learning time and professional threshold required for research and applications of LPG-SPR sensors.

2. The finite element method

The finite element method is a numerical simulation method widely used in various engineering fields. Because the detailed principles of this algorithm have already been discussed in numerous studies [11], we only provide a summary of its key content in this section. We allocated most of this section to discussing how the finite element method can be used to solve all the guided modes within the fiber structure.

The finite element method is basically a numerical solution method, and the object of its analysis is partial differential equations (PDE) with boundary conditions. This method was developed based on the variation principle, domain decomposition, and the interpolation function. The finite element method uses the variation principle (the variation algorithm) to divide the original problem (PDE with boundary conditions) into functional extreme value problems different from the original problem but with equivalent values. In other words, the same physical problem has two mathematical descriptions. That is, “boundary conditions + PDE= the functional for determining the minimum value.” After determining the functional extreme value problem equivalent to the original problem, we used the interpolation and decomposition functions for the domain we hoped to solve to convert the problem in which the functional solved for the minimum value into a set of multiple linear algebraic equations

#179197 - $15.00 USD Received 2 Nov 2012; revised 10 Jan 2013; accepted 15 Jan 2013; published 3 Jun 2013

to determine their solutions and the answer to the original problem. The calculation steps of the finite element method are briefly described with the following five points:

A. Use the equivalent functional for solving the minimum value problem to replace the PDE with boundary conditions.

B. Partition the geometric domain to be solved into several sufficiently small blocks. These blocks are known as elements, such as triangular or quadrilateral elements. The objects connecting elements are called nodes, and the unknown variable of the nodes is the desired answer.

C. One appropriate interpolation function can be used by each true function to be solved in each element for approximation. The easiest interpolation function to conduct is the linear interpolation function. Thus, the polynomial function formed by nodes can be employed for approximation of the true function to be solved in each element. This polynomial coefficient is known as the shape function.

D. Substitute this polynomial function into the functional to determine a minimum value and obtain a set of simultaneous equations.

E. Enter the boundary conditions into the simultaneous equations, and solve these equations using the Gaussian elimination method. Thus, the answer to all nodes in the domain to be solved can be obtained. After the answer to each node is obtained, each true function to be solved within the element can be further approximated using the polynomial function of the node. In other words, all unknown variables or values of the entire geometric domain to be solved can be obtained.

In this study, we used the triangular element method to cut the geometric domain of the cross-section (X-Y plane) for the fiber. The schematic diagram is shown in Fig. 3. The diagram clearly shows that the higher the cutting resolution, the more accurate the calculation results; the relative number of calculations also increases significantly. Therefore, achieving appropriate domain discretization becomes a core technique of the finite element method. As mentioned earlier, from a mathematical perspective, all theoretical modes must be pairwise orthogonals. Orthogonal value can be determined using the following equation:

$$\int_{A\infty} E_{t\nu} \times H_{t\mu} \bullet \hat{z}\, dA = \int_{A\infty} E_{t\mu} \times H_{t\nu} \bullet \hat{z}\, dA = 0 \;\; for\; \nu \neq \mu \tag{6}$$

However, numerical simulations invariably generate problems of excessive memory capacity and time requirements for mode solutions. In this study, to coordinate with the server's calculation capabilities, we examined the orthogonal values of the obtained modes to appropriately adjust the cutting resolution of the triangles. Unless otherwise noted, for this study, we used an orthogonal value of less than 10^{-4} as a guideline for all cutting resolutions.

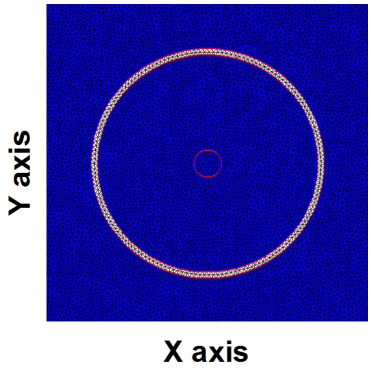

Fig. 3. The triangular cut of the fiber cross-section (X-Y plane) structure performed using the finite element method.

#179197 - $15.00 USD Received 2 Nov 2012; revised 10 Jan 2013; accepted 15 Jan 2013; published 3 Jun 2013

All guided modes within the structure could be solved after completing the cutting process, where the operating wavelength was λ = 1550 nm. Because we used a single-mode fiber, we only obtained a single-core mode (HE_{11}) with the effective refractive index n_{eff}^{core} ($n_2 < n_{eff}^{core} < n_1$), and an approximately infinite number of cladding modes with the effective refractive index $n_{eff}^{cladding}$ ($n_3 < n_{eff}^{clagging} < n_2$). Notably, the cross-sectional plane of the fiber grating previously described was uniform. Therefore, when the core mode (HE_{11}) entered the LPG domain, the mode coupling phenomenon only occurred between HE_{11} and the cladding modes of azimuthal order $l = 1$. Therefore, in this study, we focused solely on solving and exploring the $l = 1$ cladding modes. A total of 20 guided modes, including one core mode (HE_{11}) and 19 cladding modes, were solved during the preliminary process. We used the same naming convention commonly employed in fiber optics to name the 20 guided modes obtained, excluding the core mode. We then numbered the 19 cladding modes based on their effective refractive index value, where the greater the n_{eff} value was, the smaller the ν value became. Therefore, based on the value of the effective refractive index, from highest to lowest, the 19 cladding modes were represented as $\nu = 1-19$ .The finite element method can be used to obtain the core mode HE_{11} and its 2D and 3D power distribution diagrams, as shown in Fig. 4 and Fig. 5, where its effective refractive index was $n_{eff}^{core} = 1.43944$. Regarding the SPW ($\nu = 9$), its 2D and 3D power distributions are shown in Fig. 6 and Fig. 7, and its effective refractive index was $n_{eff}^{SPW} = 1.412378 + j0.0001421444$. We found that cladding mode v = 9 possessed a strong surface plasmon phenomenon, which indicated that a strong energy distribution phenomenon existed between the metallic layer and the analyte layer, as shown in Fig. 6 and Fig. 7. This type of mode is also called a surface plasmon wave (SPW). A positive correlation existed between the intensity of the surface plasmon phenomenon and its ability to detect changes in the refractive index. In other words, the stronger the surface plasmon phenomenon was, the more sensitive the sensor became. Therefore, we chose cladding mode v = 9, l = 1 as the design target of the LPG-SPR. In addition, orthogonal values among the 20 modes were calculated and examined; the results are shown in Fig. 8. Clearly, besides each mode having a self-orthogonal value of 1, the orthogonal values between two modes could satisfy the requirement of being less than 10^{-4}.

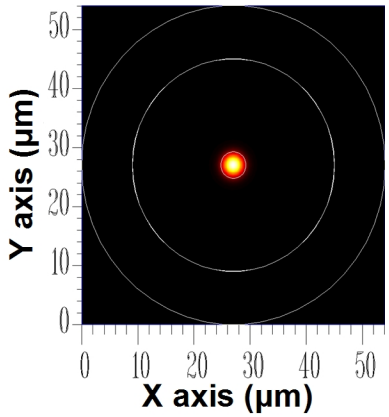

Fig. 4. The 2D power distribution of the core mode (HE_{11}) with an effective refractive index of $n_{eff}^{core} = 1.43944$.

#179197 - $15.00 USD Received 2 Nov 2012; revised 10 Jan 2013; accepted 15 Jan 2013; published 3 Jun 2013

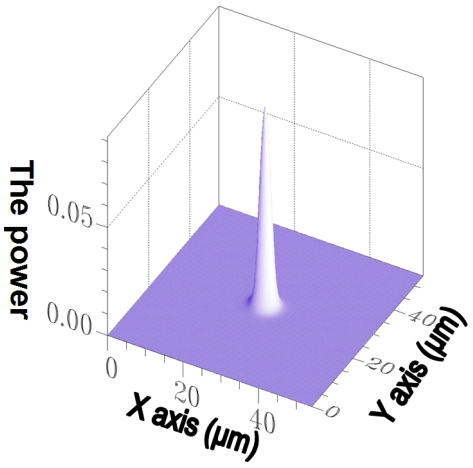

Fig. 5. The 3D power distribution of the core mode (HE_{11}) with an effective refractive index of $n_{eff}^{core} = 1.43944$.

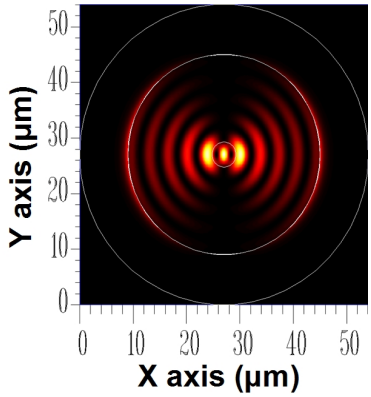

Fig. 6. The 2D power distribution of the SPW (ν = 9) with an effective refractive index of $n_{eff}^{SPW} = 1.412378 + j0.0001421444$.

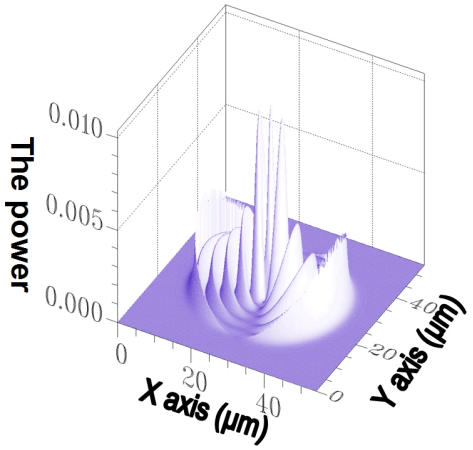

Fig. 7. The 3D power distribution of the SPW (ν = 9) with an effective refractive index of $n_{eff}^{SPW} = 1.412378 + j0.0001421444$.

#179197 - $15.00 USD Received 2 Nov 2012; revised 10 Jan 2013; accepted 15 Jan 2013; published 3 Jun 2013

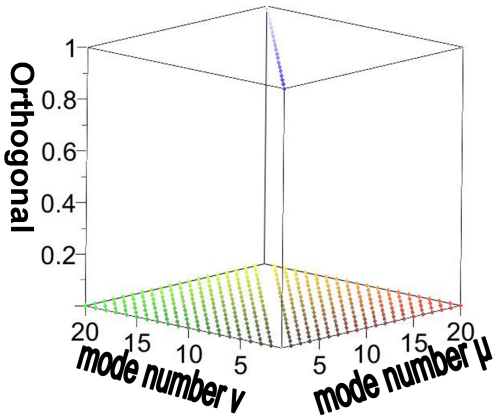

Fig. 8. The relationships between the orthogonal values of the 20 modes.

Under the simple optical fiber structure (also known as cylindrical coordinates), the analytical equations can be derived by combining Maxwell's equations with the boundary conditions, as evidenced by the complete derivation of the complex dispersion relation recorded in our previously published study [9]. By solving the complex dispersion relation, we could obtain the guided modes in the optical fiber structure. Further combining the complex dispersion relation with the Fourier series expansion (EEM), the complete computation of the LPG-SPR sensors can be indeed obtained more rapidly and accurately. However, rather than adopting the above method, we employed the FEM to determine the guided modes. The FEM was chosen for the following two main reasons: (a) Our primary goal was to use the numerical simulation technique, that is, integrate the FEM with the EEM and graphical results, to ensure that beginners in the field of LPG-SPR sensors and typical application designers don't need to face directly with numerous mathematical equations, as presented in Ref. 9. By integrating the FEM with the EEM, users can learn and design LPG-SPR sensors by using simply graphic interface. Thus, the professional requirements and skills needed to enter this field are reduced. (b) The LPG can be applied in various component designs, including fiber-grating optical add-drop multiplexers, LPG-SPR sensors, D-type LPG-SPR sensors, and crystal D-type LPG-SPR sensors. When the components to be designed possess an arbitrary shape on the X-Y plane, deriving the analytical equations using the Maxwell equations and boundary conditions is almost impossible. In other words, the analytical equations can only be employed to calculate certain geometrical structures, making them highly impractical. Therefore, to offer greater versatility in design techniques, we adopted the FEM numerical technique and the EEM for our calculations. Because the FEM numerical simulation technique can be used on the X-Y plane in waveguides for all shapes and solves every existing guided mode. This was the main reason we selected it for this study. Our goal was to propose a numerical method that can be applied generally on the design of all the periodic components, rather than the method that can only be used for shape-specific components.

3. The eigenmode expansion method

The main reason for employing this method was to allow the guided modes to conduct power transfers in LPG-SPR sensors. First, this method captured one segment object from the LPG-SPR sensor periodic object and the length of the segment object is one period of the LPG-SPR sensor periodic object, as shown in Fig. 9. The diagram clearly indicates that the LPG-SPR sensor periodic object is composed of N segment objects. The length of each segment object represents one LPG period, as well as that of the LPG-SPR periodic object. Further cutting of each segment object produces mini objects called block objects (Bk) with a length of $d\Lambda$. Each block object is considered a uniform LPG-SPR sensor waveguide possessing a fixed refractive index value in the core layer. The contact surface between block object k-1

#179197 - $15.00 USD Received 2 Nov 2012; revised 10 Jan 2013; accepted 15 Jan 2013; published 3 Jun 2013

(Bk_{k-1}) and block object k (Bk_k) is called junction k-1 (J_{k-1}), which is presented in Segment (1) of Fig. 9 and Fig. 10. The diagram clearly shows that by employing the same cutting mechanism, the block objects obtained from cutting segment object (m) and segment object (n) are identical completely. In other words, under the same cutting procedure, completing the cutting computation for a segment object equates to completing the cutting computation for an entire LPG-SPR senor periodic object. In this study, we cut a segment object into 300 uniform block objects. The eigenmode expansion method targeted one segment object from the LPG-SPR sensor periodic object and the segment was cut into 300 uniform block objects. In each block object, the guided modes that may exist were recalculated. Next, power conversions between block objects were performed using the Fourier series expansion method. The steps in this procedure can also be performed to complete the power transfers of the entire LPG-SPR sensor [12–14].

This simple description clearly indicates that for periodic components, the guided modes in each segment are the same. Therefore, using the finite element method to solve the guided modes, we only needed to complete calculations for one segment, as shown in Fig. 9. Obviously, this significantly reduces the calculation time and memory capacity required to complete the entire component simulation. Therefore, the combination of the finite element method and mode expansion method is extremely appropriate for designing components with periodic structures, such as fiber-grating optical add-drop multiplexers, LPG-SPR sensors, D-type LPG-SPR sensors, and crystal D-type LPG-SPR sensors. All the requirements for the FDTD algorithm are a light source, object cutting, boundary conditions, and Maxwell equations. By cutting objects, employing light injection, combining Maxwell equations with boundary conditions, and using previous known point, we can find the next unknown point and subsequently complete the component's simulation calculations. When λ = 1550 nm, simulating a component that was approximately 0.14 cm in length was almost impossible for FDTD. Even using a super computer, calculations for 0.1-cm to 0.2-cm sensors require unimaginable amounts of memory and computation time. By contrast, calculations using the beam propagation method still possess excessive restrictions and errors for multiple reflective 3D fiber-grating structures. The preceding descriptions clearly show that the single-period calculation characteristic is why the combination of the finite element method and the eigenmode expansion method are far superior to the finite-difference time-domain method and the beam propagation method.

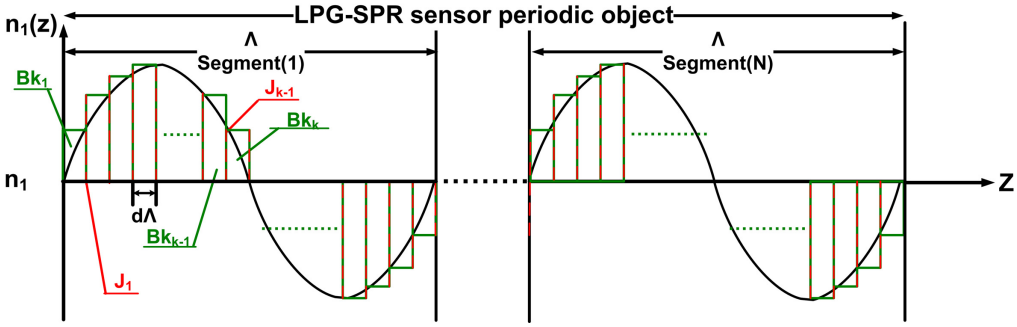

Fig. 9. Each cut block object in a segment object is considered a uniform waveguide with a fixed refractive index.

#179197 - $15.00 USD Received 2 Nov 2012; revised 10 Jan 2013; accepted 15 Jan 2013; published 3 Jun 2013

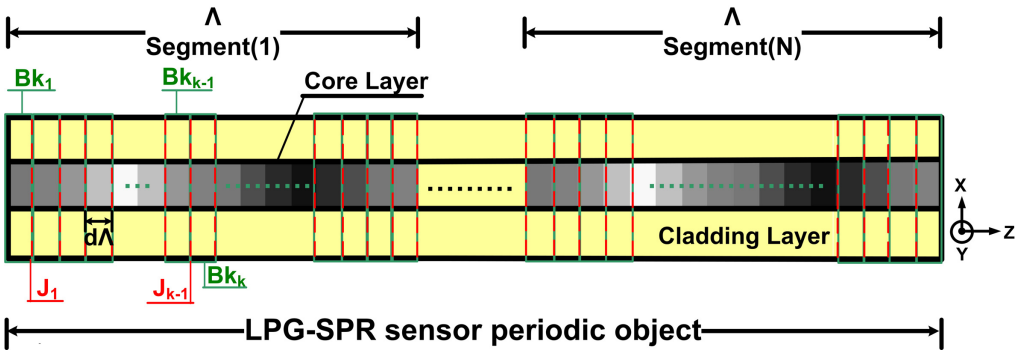

Fig. 10. Cutting schematic for the LPG propagation direction in LPG-SPR periodic object.

Next, we explain how the eigenmode expansion method was used for the LPG-SPR sensor's power propagation. Based on the preceding descriptions, for one period, the LPG-SPR sensor was cut into several uniform waveguides. For each uniform waveguide, the solution to the Maxwell equations could be considered Eq. (7). Specifically, the mode content Φ_n and the propagation constant β_n were the eigenfunction and eigenvalue obtained using the finite element method.

$$E(x,y,z) = \Phi_n(x,y)\, e^{i\beta_n z} \tag{7}$$

By combining Eq. (7) with the Fourier series expansion concept, and adding the entire forward propagation mode $Bk_k^{(+)}$, as shown in Eq. (8), and the back propagation mode $Bk_k^{(-)}$, as shown in Eq. (9), obtained using the finite element method, where $m = 20$ was the guided mode amount, and C_n^f and C_n^b were the coefficients for each forward and backward mode field, as shown in Fig. 11, the electric and magnetic fields within the uniform block object Bk_{k-1} can be obtained, as shown in Eq. (10) and Eq. (11).

$$Bk_k^{(+)} = \sum_{n=1}^{m} C_n^f \Phi_n(x,y) e^{i\beta_n z} \tag{8}$$

$$Bk_k^{(-)} = \sum_{n=1}^{m} C_n^b \Phi_n(x,y) e^{-i\beta_n z} \tag{9}$$

$$E(x,y,z) = \sum_{n=1}^{m} (C_n^f e^{i\beta_n z} + C_n^b e^{-i\beta_n z}) E_n(x,y) \tag{10}$$

$$H(x,y,z) = \sum_{n=1}^{m} (C_n^f e^{i\beta_n z} - C_n^b e^{-i\beta_n z}) H_n(x,y) \tag{11}$$

After the propagated electromagnetic fields for a uniform block object Bk_{k-1} are obtained, power must be precisely transferred from Block object Bk_{k-1} to Block object Bk_k. Here, we used the scattering matrix to transform the forward and backward power propagation of two adjacent block objects, as shown in Eq. (12). In Fig. 12, $Bk_{k-1}^{(+)}$, $Bk_k^{(+)}$ and $Bk_{k-1}^{(-)}$, $Bk_k^{(-)}$ were the total of the forward and backward propagation modes for the uniform block object Bk_{k-1} and the uniform block object Bk_k, and J_{k-1} was the scattering matrix of the adjacent block object junctions.

$$\begin{bmatrix} Bk_{k-1}^{(-)} \\ Bk_k^{(+)} \end{bmatrix} = J_{k-1} \begin{bmatrix} Bk_{k-1}^{(+)} \\ Bk_k^{(-)} \end{bmatrix} \tag{12}$$

#179197 - $15.00 USD Received 2 Nov 2012; revised 10 Jan 2013; accepted 15 Jan 2013; published 3 Jun 2013

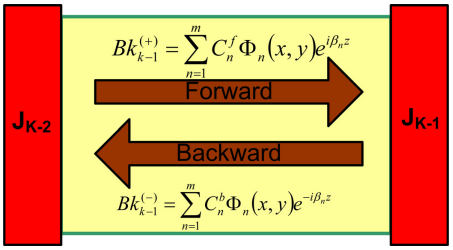

Fig. 11. Fourier series expansion for the forward and backward propagation modes.

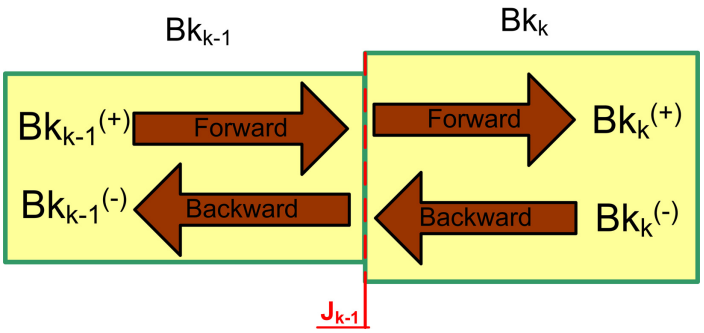

Fig. 12. The relationship between the field strength of the two adjacent uniform block objects Bk_{k-1} and Bk_k.

To convert power between adjacent block objects, we employed the Fourier series expansion to obtain the unknown junction scattering matrix J_{k-1}. Finally, the coupling effects of LPG-SPR sensors could be accurately conducted and completed by following the steps of this method. After considering detailed descriptions of the EEM, we can clearly determine that for periodic objects, only one segment object (that is, one period) is required during the cutting and mode-solving procedures. Then, by calculating each junction scattering matrix J_{k-1}, we can complete the simulation of the period object's modal transfer phenomenon. In summary, the ability to cut one single segment object and solve modes is the primary reason the EEM is superior to FDTD on calculation time and amount of memory used. In the traditional unconjugated form of coupled-mode theory, the solution calculation of the guided modes occurred only at the beginning of the X-Y cross-section, and throughout the entire process of the optical signal passing through the LPG-SPR sensor, the guided modes were never re-calculated. Therefore, the traditional unconjugated form of coupled-mode theory emphasizes that changes in the LPG induced refractive index (δn) cannot be excessive, and must generally be smaller than 3×10^{-3}. Otherwise, the traditional unconjugated form of coupled-mode theory would exhibit significant errors. Compared to the traditional unconjugated form of coupled-mode theory, the eigenmode expansion method employed in this study can detailed cut one segment into 300 uniform block objects and re-solve for the guided modes of each uniform block object. In other words, this method is not disadvantaged by requiring that the induced refractive index charge is not excessive. In addition, unless otherwise specified, all the induced refractive index changes in this study used $\delta n = 7.25 \times 10^{-3}$ as the guideline.

According to the detailed description of the eigenmode expansion method, we determined that in Eq. (8) and Eq. (9), m represents the number of guided modes and can critically affect the accuracy of the method. From a mathematical perspective, the Fourier series expansion must include all the guided modes that existed in the structure. However, this is impossible for numerical simulations because the time and memory required to perform such calculations are excessive and cannot be tolerated. However, if the number of modes is insufficient, some

#179197 - $15.00 USD Received 2 Nov 2012; revised 10 Jan 2013; accepted 15 Jan 2013; published 3 Jun 2013

power loss will occur during each pass through the scattering matrix for the adjacent block object junction. Therefore, for this study, we employed the reverse thinking method, and searched for the minimum m value that satisfied the requirement that the power loss value could not exceed 10^{-4}. Figure 13 shows the eigenmode expansion method that employed 20 guided modes (i.e., $m = 20$), and the relationship between positions and power losses of each Fourier series expansion. In this study, we uniformly cut a segment object into 300 uniform block objects. With using 300 uniform block objects and 20 guided modes, the results in Fig. 13 verify that the power loss of the EEM fully satisfied the $<10^{-4}$ criterion. Therefore, unless otherwise specified, the standard number of all guided modes used in this study was 20, and the standard number of block objects used in this study was 300.

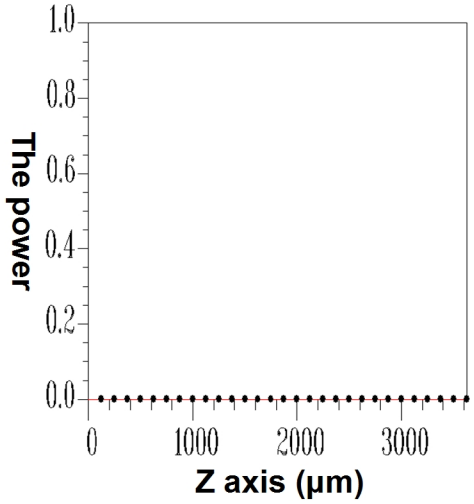

Fig. 13. The relationships between Fourier series expansion position and power loss for the eigenmode expansion method that employed 20 guided modes.

4. Design and analysis of LPG-SPR sensors

Summarizing the numerical simulation methods described in Sections 2 and 3, in this section, we developed a rigorous, simplistic, and comprehensive design process (as shown in Fig. 14), which we used to complete the analysis and design of LPG-SPR sensors. The geometric structure of the fiber used for simulation in this section is shown in Fig. 15, where L = N*Λ (μm) was the single-mode fiber with LPG. By combining the finite element method and the eigenmode expansion method, we can rapidly scan the core mode (HE_{11}) to facilitate full coupling with SPW (ν = 9) of the same propagation direction. A diagram of the relationship between transmission power and LPG periods is shown in Fig. 16. A diagram of the relationship between the transmission power and LPG period number for the core mode (HE_{11}) fully coupled to SPW (ν = 9) of the same propagation direction is shown in Fig. 17. Combining Fig. 16 and Fig. 17, we found that for period Λ = 47.57399 μm, and when the number of periods was N = 29, the core mode (HE_{11}) was fully coupled to the SPW (SPW, ν = 9) of the same propagation direction. Based on these two parameters, we inputted the core mode (HE_{11}) from the left end of Fig. 15 to observe the power propagation at the Y = 0 plane or the X-Z plane. The results are shown in Fig. 18. Evidently, under LPG disturbance, the core mode power was fully coupled to the SPW (ν = 9) of the same propagation direction during the propagation process. In addition, to verify the accuracy of mode coupling, we obtained the 2D and 3D power distributions of various z-axis positions shown in Fig. 18.

Figure 19 and Fig. 20 show 2D and 3D power distributions for SPW of z = 990 μm. Figure 21 and Fig. 22 show 2D and 3D power distributions with SPW of z = 1100 μm, respectively. Figure 23 and Fig. 24 show 2D and 3D power distributions of SPW from an

#179197 - $15.00 USD Received 2 Nov 2012; revised 10 Jan 2013; accepted 15 Jan 2013; published 3 Jun 2013

LPG-SPR sensor output, respectively. When Fig. 6 was compared to Fig. 23 and Fig. 7 was compared to Fig. 24, their graphical similarity verified that the methods proposed in this study were correct. In addition, to comply with the design process norm of Step 2, the orthogonal values of this sample were calculated and verified; the results are shown in Fig. 25. Besides having the self-orthogonal value of 1 for each mode, the orthogonal values between two modes can satisfy the requirements of being less than 10^{-4}. Obviously, the propagation distance and power loss conditions of this example must also be examined. As shown in Fig. 26, the power loss can satisfy the less than 10^{-4} requirement specified in Step 3 of the design process.

In traditional coupled-mode theories [15,16], to obtain an exact solution, numerous approximations and assumptions must be employed when developing the equation; for example, $\delta n << n_1$, ignoring the longitudinal coupling coefficient $K_{\nu-\mu}^{z}$, and the assumption that the simultaneous power coupling phenomenon can only occur between two modes. Thus, Eq. (2) is simplified into a two-mode coupled-mode equation. Therefore, referencing studies [15] and [16], we found that the designed wavelength λ_D and the maximum reflection wavelength $\lambda_{\max}$ produce inconsistent phenomena.

Regarding the design process proposed in this study (Fig. 14), the setting of $\lambda_D = 1550nm$ was finished in Step 1 and all design steps were completed based on this wavelength. The LPG period and period numbers required were determined in Step 4. The LPG parameters required by the core mode (HE_{11}) fully coupled to the SPW ($\nu = 9$) of the same propagation direction were $\Lambda = 47.57399$ μm and $N = 29$. We calculated the spectrum graph, and the results are shown in Fig. 27. From this figure, we found that the maximum transmission wavelength $\lambda_{\max}$ was accurate to our original design, that is, $\lambda_D = 1550nm$.

When evaluating the advantages and disadvantages of various sensors, the resolution and sensitivity are two critical indicator parameters that must be considered. The resolution significantly affects identification of the positions where the SPW resonance wavelength occurred using an optical spectrum analyzer (OSA), and sensitivity is the response level expressed when analytes sense or detect parameter change. In layman's terms, resolution is the depth of the resonance wavelength occurrence points in the sensor spectral graph, and sensitivity is the size of the shifts in the resonance wavelength occurrence points. To understand the sensor's resolution and sensitivity levels, we changed the analyte refractive index from 1.395 to 1.405. We increased the index by 0.001 for each adjustment to observe the conditions of resonance wavelength shifts; the results are shown in Fig. 28. At the design point of $n_4 = 1.4$, the sensor had a resolution of approximately −45 dB. Based on Fig. 28, we corresponded the resonance wavelength to the analyte refractive index n_4; the results are shown in Fig. 29. Using Fig. 29, we can easily calculate that the sensor had a sensitivity of approximately 27000 nm/RIU (refractive index unit). The analyte refractive index changes and resonance wavelength shift directions can be reasonably explained using the approximate Eq. (13) shown below.

$$\lambda_D = \lambda_{\max} \cong \left[n_{eff}^{core} - \mathrm{Re}(n_{eff}^{SPW}) \right] \cdot \Lambda . \tag{13}$$

For the Eq. (13) in the spectral graph, the LPG period (Λ) is a fixed constant. Therefore, the various positions of the SPW that appeared in the spectrum graph ($\lambda_D = \lambda_{\max}$) were directly and inversely proportional (because it possessed a minus sign in the Eq. (13) to the effective refractive index $\mathrm{Re}(n_{eff}^{SPW})$ of the SPW. When the refractive index of the analyte increased, the effective refractive index of the SPW also exhibited growth. That is, when we changed the analyte refractive index from 1.395 to 1.405 (from small to large), the resonance wavelength in the spectrum graph shifted from the right to the left.

#179197 - $15.00 USD Received 2 Nov 2012; revised 10 Jan 2013; accepted 15 Jan 2013; published 3 Jun 2013

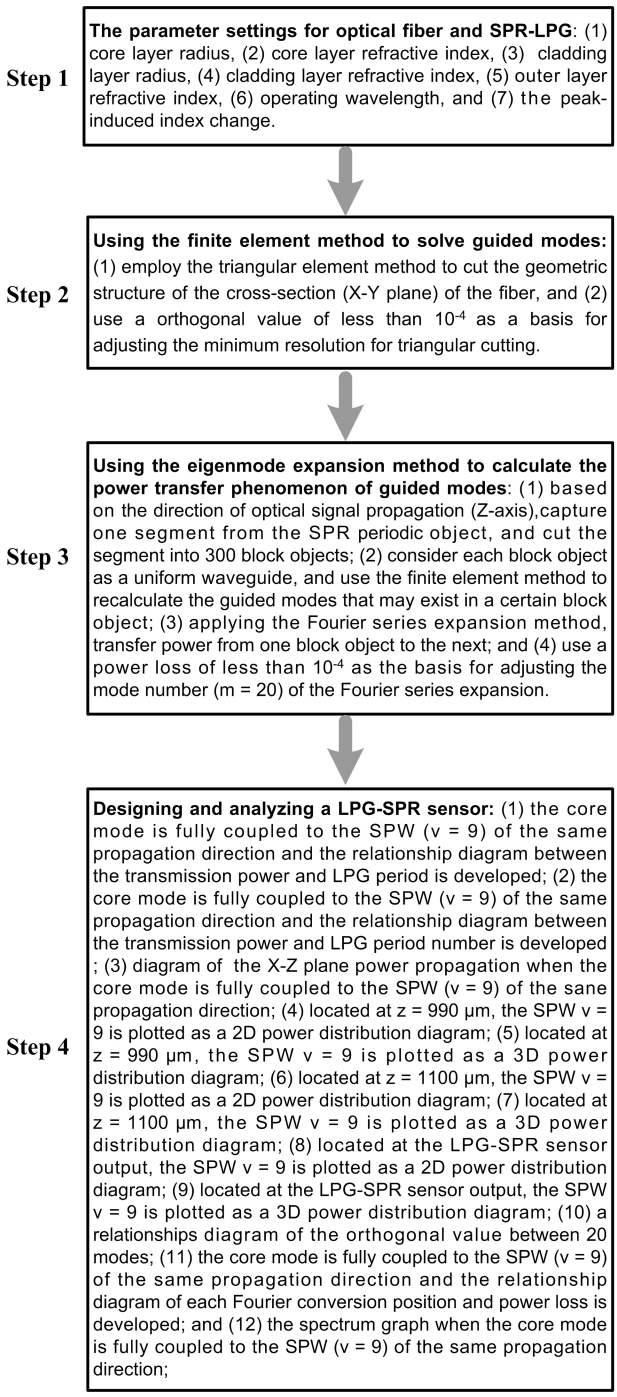

Fig. 14. Flowchart of the LPG-SPR sensor design and analysis.

#179197 - $15.00 USD Received 2 Nov 2012; revised 10 Jan 2013; accepted 15 Jan 2013; published 3 Jun 2013

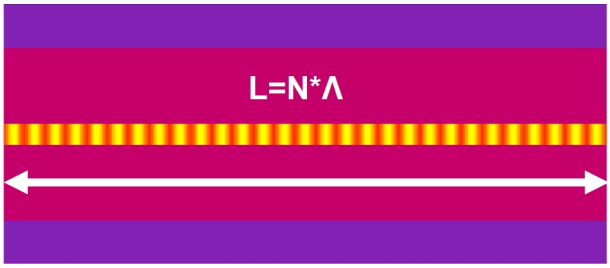

Fig. 15. The X-Z plane geometric structure of LPG-SPR sensor.

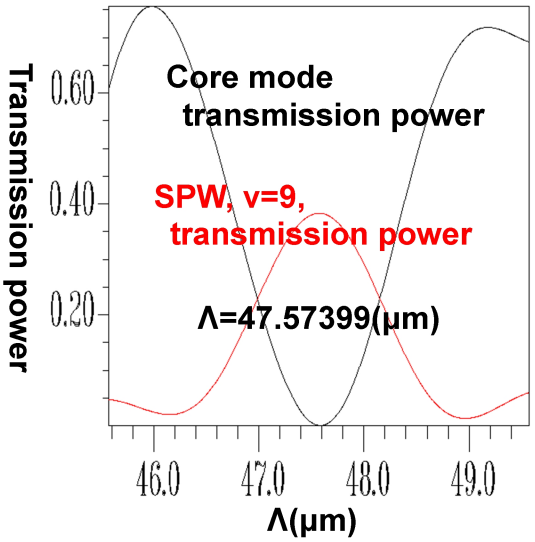

Fig. 16. The transmission power and LPG period relationship of the core mode fully coupled to SPW, ν = 9, of the same propagation direction.

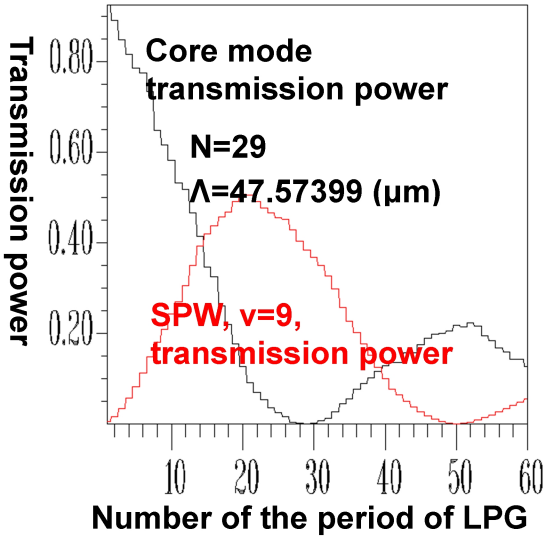

Fig. 17. The transmission power and LPG period number relationship of the core mode fully coupled to the SPW, ν = 9, of the same propagation direction.

#179197 - $15.00 USD Received 2 Nov 2012; revised 10 Jan 2013; accepted 15 Jan 2013; published 3 Jun 2013

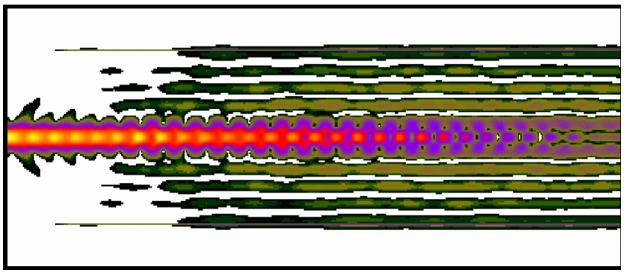

Fig. 18. The X-Z plane power transmission of the core mode fully coupled to the SPW, ν = 9, of the same propagation direction.

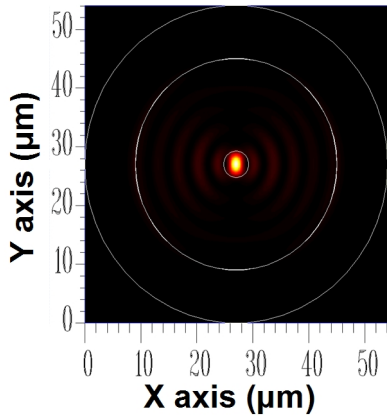

Fig. 19. The 2D power distribution of the SPW at z = 990 μm.

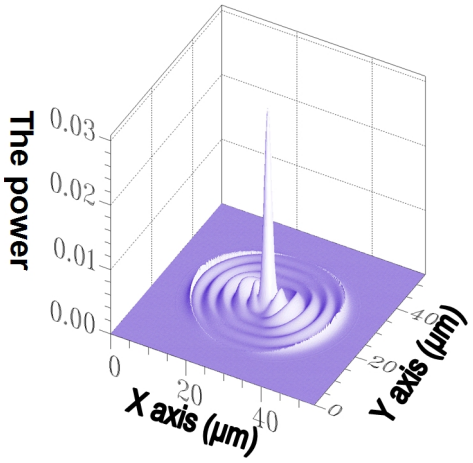

Fig. 20. The 3D power distribution of the SPW at z = 990 μm.

#179197 - $15.00 USD Received 2 Nov 2012; revised 10 Jan 2013; accepted 15 Jan 2013; published 3 Jun 2013

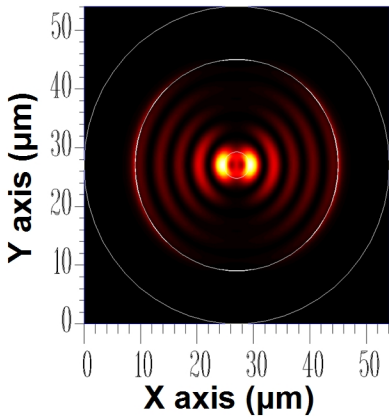

Fig. 21. The 2D power distribution of the SPW at z = 1100 μm.

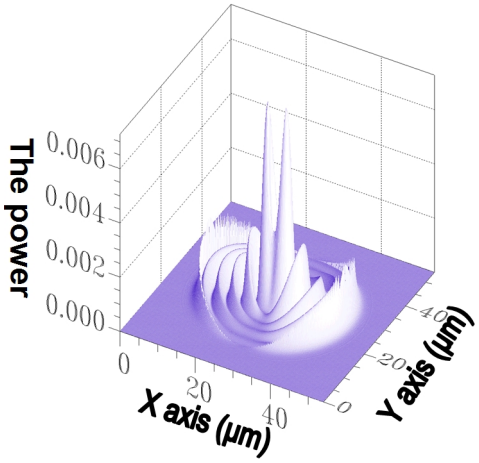

Fig. 22. The 3D power distribution of the SPW at z = 1100 μm.

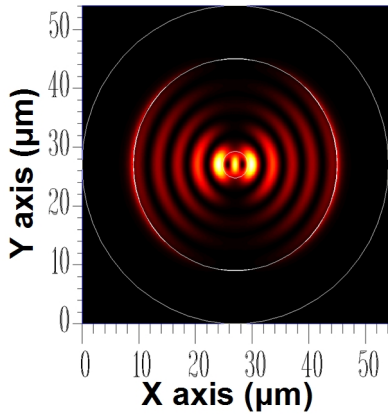

Fig. 23. The 2D power distribution of the SPW at z = 1379.64571 μm.

#179197 - $15.00 USD Received 2 Nov 2012; revised 10 Jan 2013; accepted 15 Jan 2013; published 3 Jun 2013

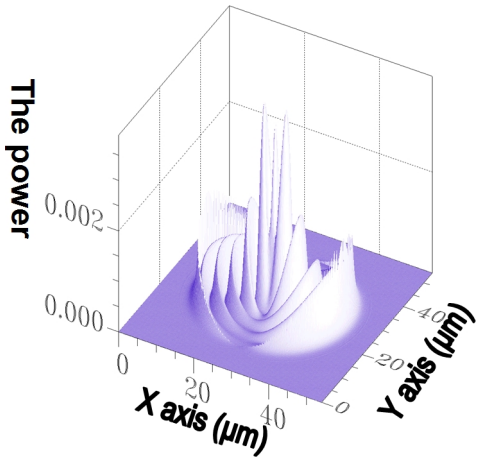

Fig. 24. The 3D power distribution of the SPW at z = 1379.64571 μm.

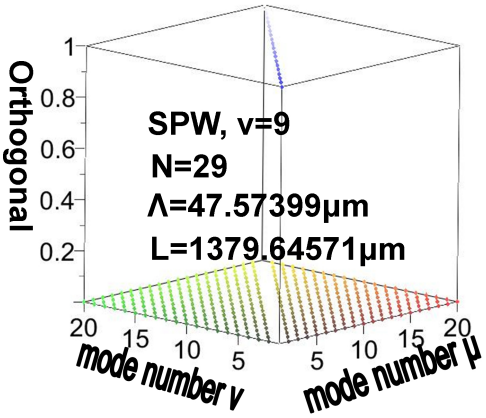

Fig. 25. The relationships between the orthogonal values of the 20 modes.

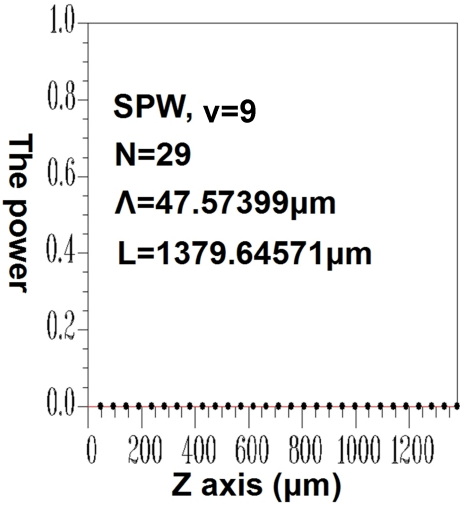

Fig. 26. The relationships between the Fourier series expansion positions and power losses of the core mode fully coupled to the SPW, ν = 9, of the same propagation direction.

#179197 - $15.00 USD Received 2 Nov 2012; revised 10 Jan 2013; accepted 15 Jan 2013; published 3 Jun 2013

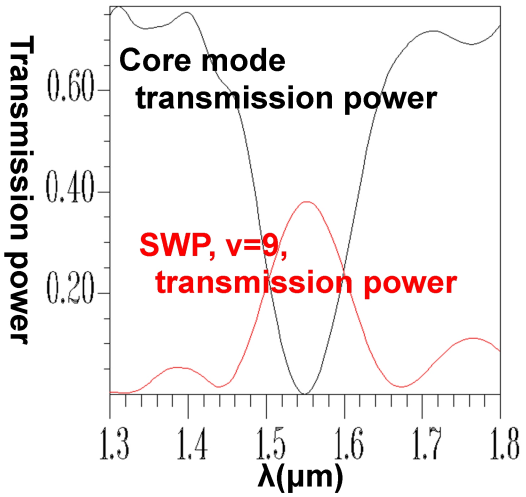

Fig. 27. Spectrum graph of the core mode fully coupled to the SPW, ν = 9, of the same propagation direction.

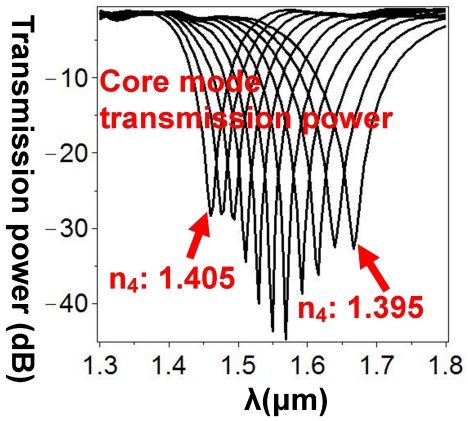

Fig. 28. Spectrum changes for the SPW, ν = 9, of the same propagation direction when the analyte refractive index n_4 changed.

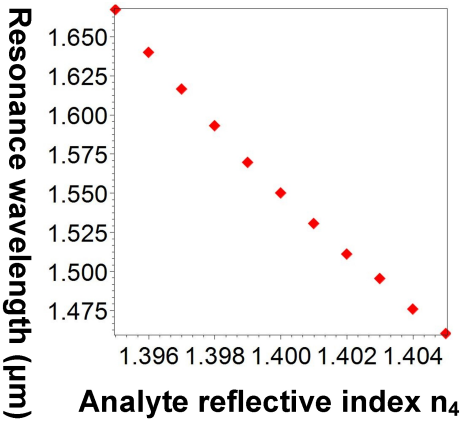

Fig. 29. The relationships between the analyte refractive index n_4 and the SPW's resonance wavelength.

#179197 - $15.00 USD Received 2 Nov 2012; revised 10 Jan 2013; accepted 15 Jan 2013; published 3 Jun 2013

5. Conclusion

In this study, we combined the finite element method and the eigenmode expansion method, as well as a rigorous, simplistic, and comprehensive design process, to propose a visual, graphic, and simplistic numerical simulation method for designing and analyzing LPG-SPR sensors. For LPG-SPR sensors approximately 0.1 cm to 0.2 cm in length, no numerical simulation methods currently exist to conduct 3D component analysis and design. In Section 3, we thoroughly explained why the mode expansion method required less memory and time to complete large-scale LPG-SPR sensor analysis and design. We extracted single period objects from the periodic components and recalculated solutions, which is the essence of the entire eigenmode expansion method. This section showed the distinctiveness and unique features of this study. In Section 4, we presented another of the most critical core techniques employed in this study. Many rigorous graphical results based on the proposed design flow were also shown in this section. The goal was to enable novice learners or application-level designers new to the field of LPG-SPR sensors to use an easier graphical method when learning about the traditional unconjugated form of coupled-mode theory, and to minimize the likelihood of encountering formulaic and abstract mathematical models directly. Notably, compared to the traditional coupled-mode theory, the maximum transmission wavelength $\lambda_{\max}$ of the LPG-SPR sensor constructed following the design flow proposed in this section was accurate to the pre-planned design wavelength λ_D . Additionally, the power loss condition and mode orthogonal values were calculated and verified using examples to ensure that they conformed to design process specifications. We confirmed that the LPG-SPR sensor designed in this study possesses a resolution of ~-45 dB and a sensitivity of ~27000 nm/RIU (refractive index unit). The goal of this study was to supplement the traditional unconjugated form of coupled-mode theory with rigorous, simplistic, and graphical numerical techniques to reduce the complexity and difficulty of understanding LPG-SPR sensors.

Acknowledgment

The author gratefully acknowledges the support provided to this study by the National Science Council of Taiwan (NSC101-2622-E-007-CC3).

#179197 - $15.00 USD Received 2 Nov 2012; revised 10 Jan 2013; accepted 15 Jan 2013; published 3 Jun 2013